Numerical Methods in Civil Engineering, 8-4 (2024) 54-67

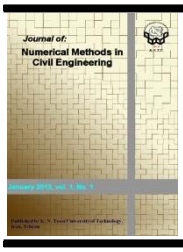

Numerical Methods in Civil Engineering

Journal Homepage: https://nmce.kntu.ac.ir/

Comparative Performance Assessment of RCS Connections According to Different Generations of ASCE Guidelines

Elmira Tavasoli Yousefabadi*, Mohammad Taghi Kazemi **

ARTICLE INFO

RESEARCH PAPER

Article history:
Received:
April 2024
Revised:
June 2024
Accepted:
July 2024

Keywords:
Composite structures,
RCS joints,
Cyclic loading,
Finite element method,
Seismic performance

Abstract:

The hybrid moment-resisting frames, comprising Reinforced Concrete columns and Steel beams (RCS), have attracted attention due to potential cost savings and enhanced structural characteristics. The ASCE Task Committee on Design Criteria for Composite Structures issued early guidelines for RCS joint design, primarily applicable to low seismicity regions. Subsequent research has demonstrated the reliable ductile performance of Composite RCS systems, making them attractive for high seismic areas. Following this, an updated Pre-Standard for the Design of RCS connections was introduced, serving as the latest ASCE guideline for designing RCS joints. This paper investigates the cyclic performance of different RCS joint details, focusing on the influence of design requirements on connection behavior. Four specimens are selected for investigation, with two conforming to the early ASCE guideline and two to the updated ASCE guideline. The early ASCE guideline-conforming specimens closely resemble the updated ones, with the distinction that a doubler plate is attached to their beam web. A detailed finite element model, validated against experimental data, is employed to analyze the specimens. The results indicate better connection performance when adhering to the early ASCE guideline requirements compared to the updated ASCE guideline. The incorporation of a 6 mm thick doubler plate, along with four triangular stiffeners, significantly enhances connection performance, including increased initial strength, reduced strength degradation, and improved energy dissipation capacity. These modifications contribute minimally to the overall building cost while yielding a substantial 25.5% increase in connection energy dissipation capacity and a 40% reduction in strength deterioration during cyclic loading.

1. Introduction

In recent decades, there has been a significant focus on employing hybrid moment-resisting frames in building construction, particularly those incorporating Reinforced Concrete columns and Steel beams (RCS). This structural system has attracted attention due to its potential for material cost savings and enhanced structural characteristics. RCS frames optimize the use of both steel and concrete materials. The adoption of RC columns, known for their superior compressive performance and stability contribute to increased structural damping and lateral stiffness, thereby improving seismic resistance. Incorporating steel beams amplifies the ability to dissipate energy and enhance ductility. Additionally, RCS frames offer advantages such as feasibility in construction, the ability to implement beams with long spans, reduced floor weight, and adherence to the strong column–weak beam criterion. The economic benefits of utilizing concrete columns, especially in high-rise buildings where stiffness is a primary concern, make RCS frames a viable choice in seismic regions. The primary challenge in RCS system design is comprehending the interaction between the steel beam and the RC column. Numerous research projects have delved into investigating the seismic behavior of RCS connections [1], [2]. Notably, A thorough testing initiative was carried out at the University of Texas at Austin [3], [4]. The test specimens involved through-beam connections, where steel beams pass through RC columns and are subjected to nonlinear monotonic and cyclic loads. Based on the findings of these studies, in 1994, the American Society of Civil Engineers (ASCE) Task Committee [5] developed design guidelines

* *Corresponding Author: PhD Candidate of Civil Engineering, Sharif University of Technology, Kish International Campus, Kish Island, Iran. E-mail: tavasoli_elmira@kish.sharif.edu*

** *Associate Professor of Department of Civil Engineering, Sharif University of Technology, Tehran, Iran. E-mail: kazemi@sharif.edu*

https://doi.org/10.61186/NMCE.2404.1052

for RCS connections in structures experiencing low to moderate earthquake hazards.

Following the 1994 ASCE Guideline, researchers in the United States and Japan conducted thorough studies on RCS systems as part of a collaborative research program on composite construction. Noteworthy contributions include works by Kanno and Deierlein [6], [7], Parra-Montesinos and Wight [8], Bugeja et al. [9], and Noguchi and Kim [10]. Several proposals have emerged, incorporating advancements to more accurately capture the anticipated strength and stiffness of composite joints, as evidenced by works such as those by Kuramoto and Nishiyama [11] and Parra-Montesinos et al. [12].

The research conducted has led to significant enhancements to the 1994 ASCE Guideline. These improvements encompass validation and extension of the guidelines for application in high seismic zones, a reduction in transverse tie requirements within joint height, expansion of the original model to encompass a broader range of joint details, modifications to address distinctions between interior and exterior joints, permission for the use of high-strength concrete, and the incorporation of performance-based requirements aimed at limiting anticipated deformation and damage. The 2015 ASCE Pre-standard [13] was developed as an enhanced edition of the 1994 ASCE Guideline. The 2015 revision builds upon and enhances the previous guideline, incorporating newer experimental studies and research findings related to cyclic load conditions, employing high-strength concrete, alternate joint configurations, and enhanced design concepts. In alignment with the AISC 341 [14], the 2015 Pre-Standard mandates that beam-column joints anticipate enduring a minimum story drift ratio of 0.04.

Moreover, numerous experimental studies carried out in recent years have focused on RCS joints intending to develop enhanced joint details. Specifically, Alizadeh et al. [15], [16] incorporated extended bearing plates and self-consolidating concrete to enhance joint strength, and energy dissipation capacity, and facilitate construction. Mirghaderi et al. [17], Eghbali and Mirghaderi [18], as well as, Nguyen et al. [19] proposed innovative joint details involving the use of cover plates in beam flanges and vertical plates in the joint region. Park et al. [13] demonstrated the viability of concrete-filled U-shaped steel beams. The performance of precast reinforced concrete columns in interaction with steel beams was examined by Khaloo and Bakhtiari Doost [20], [21]. These studies delved into the cyclic loading, stability, and displacement characteristics of RCS connections, showcasing gradual stiffness degradation, stable behavior, and increased flexibility observed in various scenarios. Such findings contribute to a broader understanding of the seismic behavior of RCS joints, offering valuable considerations for designing resilient and ductile structures in earthquake-prone regions. Novel joint configurations and construction techniques, such as high-strength bolted-end plate connections by Chen et al. [22], RCS connection with replaceable members by Men et al. [23], demountable joints developed by Li et al. [24], concentric and eccentric "New-RCS" through-beam connections by Ou et al. [25], semi-rigid prefabricated RCS connections by Pan et al. [26], and simplified connection details by Lee et al. [27], aim to enhance construction speed, reducing manufacturing difficulties, and improving overall seismic performance of RCS joints.

In addition to the experimental efforts, Numerous studies have focused on numerically simulating the behavior of RCS connections through finite element approaches, utilizing software tools such as ABAQUS [28], as referenced in [29], [30], [31], [32]. In these investigations, a finite element model for the RCS connection was developed and its accuracy was confirmed via experimental testing. Innovative connection details were then introduced, with subsequent evaluation of their performance and provision of recommendations for enhancing seismic resilience. Moreover, specific research endeavors involved conducting parametric studies, utilizing validated finite element models to explore how joint configurations affect connection performance [33], [34], [35], [36].

The present research investigates and compares the seismic behavior of different joint details designed according to the 1994 ASCE Guideline and 2015 ASCE Pre-standard, using validated finite element models. Overall, the design requirements, including limit states to be controlled, load transfer mechanisms, and allowable joint configurations, are consistent between the two sets of guidelines. Nevertheless, notable differences emerge in the equations used to calculate both the strength and stiffness of the connection, along with the criteria for proportioning structural steel and reinforcing bar details. These variations stem from the fact that the design criteria of the updated guideline are less stringent due to a better understanding of the joint behavior. The current study involves designing four specimens following both guidelines and subsequently examining the seismic performance of the specimens. To achieve this, the relationships for calculating joint strength proposed by the two guidelines are first compared. Afterward, a comprehensive finite element model is constructed and verified using experimental results obtained earlier. Four connection specimens are then designed based on the 1994 ASCE Guideline and 2015 ASCE Pre-standard. Finite element models are developed for each specimen, and the models are analyzed under cyclic loading conditions. Finally, by examining the results, suggestions for improving the RCS connection design guidelines are provided.

2. Design Requirements of RCS Joints

Two primary failure modes have been identified for an RCS connection: (1) panel shear and (2) vertical bearing failure modes. Panel shear failure resembles the shear failure observed in steel or reinforced concrete moment-resisting frames. In such connections, both structural steel and reinforced concrete elements play a role in resisting shear forces. Vertical bearing failure happens when the concrete in the column, both above and below the steel beam, is crushed, permitting the beam to rotate within the reinforced concrete column [3]. The 2015 Pre-standard aims to enhance the accuracy and consistency in predicting the strength of joints in both panel shear and vertical bearing. This guideline now encompasses a broader range of joint details that have proven effective in maintaining the strength and stiffness of composite joints while also improving constructability. Additionally, new "phi-factors" have been suggested using the beta-reliability method, the same technique used in the AISC-LRFD [37]. In the Load and Resistance Factor Design (LRFD) method, phi-factors (ϕ-factors) are resistance factors used to account for the uncertainties in the material properties, dimensions, and the assumptions made in the design equations. These factors reduce the nominal resistance to a level that provides a consistent and reliable safety margin. Each type of material or structural component has its specific ϕ-factor, which reflects its variability and reliability.

As in the 1994 Guideline, the 2015 Pre-standard will focus only on the "through-beam" type of connection. In the through-beam configuration, the steel beam remains continuous, whereas in the through-column arrangement, the concrete column is continuous. The through-beam type exhibits greater ductility and reliability, while the through-column type demands meticulous attention during construction to guarantee satisfactory ductility and strength capacity. Figure 1 depicts the components of the through-beam RCS joint, including face-bearing plates, steel band plates, steel doubler plates, and ties. It is recommended that the face-bearing plates match the width of the beam flange in all connections, as studies have shown their effectiveness in enhancing joint performance by containing concrete in the panel zone. Similarly, the steel band plates aid in concrete confinement both above and below the panel zone. The following discusses the proposed relationships of the two guidelines for determining joint shear strength, encompassing panel shear and vertical bearing mechanisms.

2.1 Effective Joint Width

The effective width of the joint within the column (b_j) is determined by summing up the widths of the inner and outer panels (b_i and b_o), expressed as:

$$b_j = b_i + b_o \tag{2}$$

The 1994 Guideline recommends that the inner width, b_i, be set equal to the wider of either the width of the Face Bearing Plate (FBP), b_p, or the width of the beam flange, b_f. In contrast, the 2015 Pre-Standard does not acknowledge this additional width and sets the inner panel width equal to the width of the beam flange.

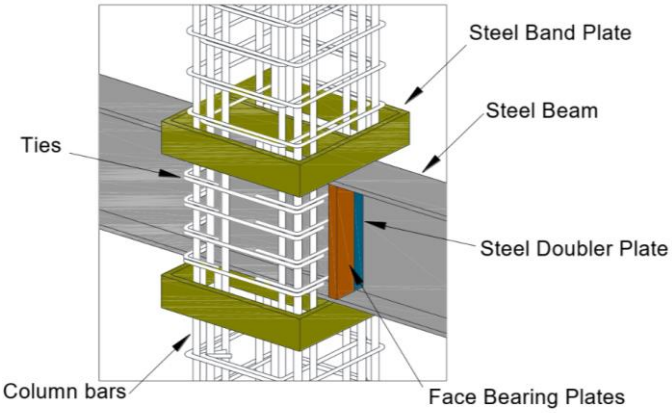

Fig. 10: Sample details of a through-beam RCS joint

The 1994 Guideline defines the outer joint width, b_o, as a ratio based on the average of the beam flange width and the column width, depending on the types of shear key employed in the joint. In contrast, the 2015 Pre-Standard takes into account larger effective joint regions. The comparison of the outer joint width, b_o, recommended by the two guidelines is outlined as follows:

1994 Guideline

$$\begin{aligned} b_o &= C(b_m - b_i) \le 0.5 d_b \\ C &= (x/h)(y/b_f) \\ b_m &= (b_f + b)/2 < b_f + h < 1.75 b_f \end{aligned} \tag{3}$$

2015 Pre-Standard

$$b_o = y + 2/3\alpha_x x - b_f \le b - b_f \tag{4}$$

in which, C represents the joint mobilization coefficient, b_m denotes the joint effective width, d_b denotes the beam depth, b_f is the beam flange width, h is the depth of the concrete column parallel to the steel beam, b is the width of concrete column, and x and y represent the effective dimensions of shear keys. When steel band plates substitute reinforcing bar ties in the bearing region above and below the beam, the value of α_x is set to 0.5; otherwise, when ties are present, α_x is set to 1.0. This distinction arises from the fact that the determination of joint width in the 1994 Guideline primarily relied on criteria for reinforced concrete joints.

2.2 Joint Strength

The shear strength of the connection is determined by adding the shear capacity of the inner panel (Vin), comprising contributions from the steel web panel and an inner concrete strut to the shear capacity of the outer concrete panel (Von). These values are then multiplied by the respective resistance factors. The components contributing to the design shear strength have undergone refinement in the 2015 Pre-Standard. While the 1994 Guideline incorporates two distinct strength criteria—panel shear and vertical bearing strength—the 2015 Pre-Standard simplifies the requirements by focusing solely on the panel shear strength criteria and limiting the nominal vertical bearing strength value. As per the 2015 Pre-Standard, the connection shear strength is deemed sufficient if only Equation (6) is met, while according to the 1994 Guideline, Equations (4) and (5) must be satisfied concurrently.

In the 1994 Guideline, joint bearing strength is treated as a distinct failure mode, separate from joint shear strength failure. It is computed and checked against the relevant design forces using Equation (5). In contrast, the 2015 Pre-Standard assumes that vertical bearing failure occurs solely over the inner panel width, bi, with the outer panel more prone to failure in outer panel shear. However, empirical test data indicates that the outer panel fails similarly regardless of whether the inner panel fails in joint shear or vertical bearing. Consequently, the 2015 Pre-Standard restricts the amount of shear developed in the inner panel by the vertical bearing strength, as illustrated in Equation (7).

The shear strength phi-factor (φs) in the 2015 Pre-Standard has been increased from the original 0.7 to 0.85. Additionally, a new strength adjustment factor, k = 0.85, has been incorporated into the design check to restrict connection deformations. In the 2015 Pre-Standard, the phi factor (φs) in Equation (6) varies based on the governing mode of failure, with φs = 0.85 for shear and φb = 0.75 for bearing. These variations in phi-factors reflect the preference for designing the joint to fail in shear, aiming to avoid the undesirable pinched response associated with bearing failure.

1994 Guideline

Panel Shear Strength Criterion:

$$V_j \le \phi(V_{in} + V_{on}) \qquad \phi = 0.7 \tag{5}$$

Vertical Bearing Strength Criterion:

$$\sum M_c + 0.35\,h\,\Delta V_b \le \phi_b M_{vb} \tag{5}$$

2015 Pre-Standard

Panel Shear Strength Criterion:

$$V_j \le k(\phi V_{in} + \phi_s V_{on}) \qquad \begin{cases}\phi_s = 0.85\\ \phi_b = 0.75\end{cases},\ \phi = \phi_s \text{ or } \phi_b,\ k = 0.85 \tag{6}$$

Vertical Bearing Strength Limit:

$$\left(\phi V_{in}\right)_{\text{Limit}} = \phi_b (M_{vb} - V_b h)/d_j \tag{7}$$

In the given expressions, V_{in} represents the shear capacity of the inner panel, V_{on} denotes the shear capacity of the outer concrete panel, V_j signifies the joint shear demand imposed by adjacent beams and columns calculated by $V_j = \sum M_b / d_j - V_c$, $\sum M_b$ and $\sum M_c$ denote the summation of beam and column moments transferred into the joint, d_j represents the effective joint depth, defined as the distance between the centerlines of the steel beam flanges, V_c represents the average column shear, V_b represents the average beam shear, ΔV_b stands for the difference in beam shears, M_{vb} represents the moment derived from the joint vertical bearing capacity, and remaining terms maintain their definitions as previously specified.

The inner panel shear capacity, V_{in}, comprises the shear capacity of the steel web panel, V_{sp}, and the inner concrete strut, V_{ic}. The prescribed methods for determining the inner panel shear capacity as recommended by each set of guidelines are outlined as follows:

1994 Guideline

$$V_{in} = V_{sp} + V_{ic} \tag{8}$$

$$V_{sp} = 0.6 F_{ysp} t_{sp}\, jh \tag{9}$$

$$V_{ic} = 1.7\sqrt{f_c'}\, b_p h \le 0.5 f_c' b_p d_w \tag{10}$$

2015 Pre-Standard

$$\phi V_{in} = \phi_s (V_{sp} + V_{ic}) \tag{11}$$

$$V_{sp} = 0.6 F_{ysp} t_{sp} \alpha_{sp} h \tag{12}$$

$$V_{ic} = 1.7\alpha_c \sqrt{f_c'}\, b_i h \le 0.5 f_c' b_f d_j \tag{13}$$

Here, F_{ysp} stands for the yield strength of the steel panel, while t_{sp} represents its thickness. The coefficients α_{sp} are set at 0.9 for interior connections and 0.8 for exterior connections. The parameter jh is the horizontal distance between the bearing force resultant, with consideration that it should be $\le 0.7h$, where h represents the concrete column depth. The coefficients α_c are assigned values of 1.0 for

interior connections and 0.6 for exterior connections, with f'_c representing the concrete compressive strength in MPa. The nominal capacity of the outer diagonal concrete strut, V_{on}, is specified by each guideline as follows:

1994 Guideline	
$V_{on} = 1.7\sqrt{f'_c}\, b_o h$	(14)
2015 Pre-Standard	
$V_{on} = 1.25\alpha_c \sqrt{f'_c}\, b_o h$	(15)

where α_c retains its previous definition as described for the inner panel in Equation (13), and the remaining terms maintain their previously defined meanings.

3. FE Modeling and Validation

3.1 Experiment Description

The validated numerical model of RCS connections implemented in this study was assessed through an experimental test carried out by Alizadeh et al. [15]. The selected specimen consisted of a reinforced concrete (RC) column measuring 3,150 mm in height, featuring a square cross-section (400 × 400 mm) and connected to two steel IPE300 beams, each spanning 1,730 mm. A visual depiction of the experimental setup is provided in Figure 2. As shown in the illustration, simple supports were utilized at the ends of the steel beams. The bottom end of the concrete column was connected to the base with a pin-type connection support. Two hydraulic jacks were placed at the column's top to apply reversed lateral cyclic loading.

A constant axial force of 300 kN was exerted at the top of the column, amounting to roughly 4% of the column's total axial strength. To prevent any lateral movements out of the specified plane during the test, lateral bracing was provided at both ends of the beams and columns. The loading sequence comprised 22 cycles, beginning at 0.2%, followed by drift ratios of 0.25%, 0.375%, 0.5%, 0.75%, 1%, 1.5%, 2%, 3%, 4%, 5%, and 6%. Notably, the cycles with drift ratios ranging from 0.25% to 4% were repeated twice (see Fig. **12**).

3.2 FE Model

The selected specimen is simulated using ABAQUS [28]. Steel beams and concrete columns are modeled using 8-node solid elements, specifically the C3D8R element in ABAQUS. The C3D8R element in ABAQUS is an eight-node linear brick element with reduced integration and hourglass control. Its advantages include reduced computational resources, efficient performance, and built-in hourglass control to improve accuracy.

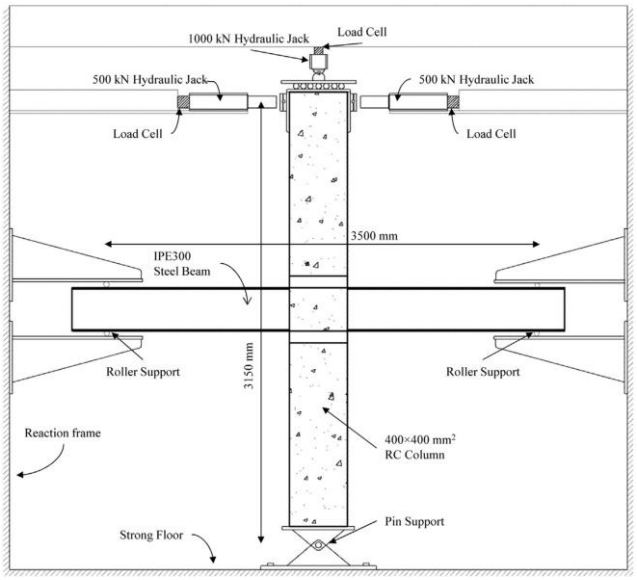

Fig. 11: Configuration of test setup conducted by Alizadeh et al. [12]

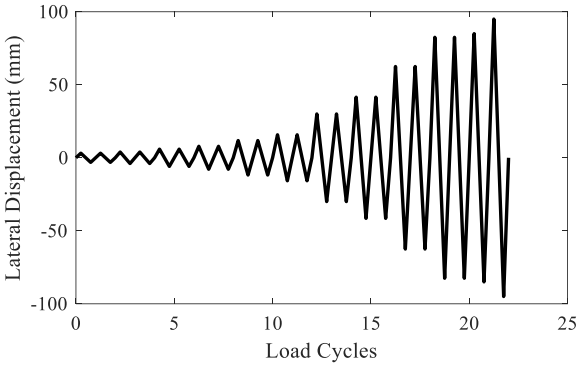

Fig. 12: Cyclic loading protocol

It is versatile for various analyses, handles nonlinear behavior and large deformations well, and tolerates poor mesh quality. Additionally, C3D8R elements are user-friendly and suitable for complex models, offering a good balance between accuracy and efficiency. Steel rebars are represented by truss elements, specifically the T3D2 element, and they are considered fully embedded within the concrete. Following a parametric study, a mesh size of 20 mm was determined to be sufficient for accurately capturing the joint behavior in the model. The resulting finite element model is depicted in Fig. **13**.

To improve the simulation of the interaction between steel and concrete, the model enables the separation of the steel beam and concrete column at the joint region. The analysis involves two steps: initially, an axial load simulating gravity loads is imposed, followed by lateral loading of the column as per the predefined loading protocol.

The constraint used for the interaction between the steel reinforcements and the concrete column is the “Embedded” constraint. In ABAQUS, the assumptions of the “Embedded” constraint are set as default. The weld joint is

simulated using the "Tie" constraint. The "Surface to surface" contact is employed for contact pairs such as plate-to-plate and bolt-to-plate.

The isotropic von Mises yielding criterion describes the constitutive behaviors of the bolt, steel, and reinforcement. The concrete's plasticity and damage characteristics are captured by the damage plasticity model in ABAQUS. The parameters for this model are configured as follows: a dilation angle of 30 degrees, an eccentricity of 0.1, an fb0/fc0 ratio of 1.16, a K value of 0.667, and a viscosity parameter of 0.0001. The Poisson's ratio for concrete is set to 0.2, with a density of 2400 kg/m³.

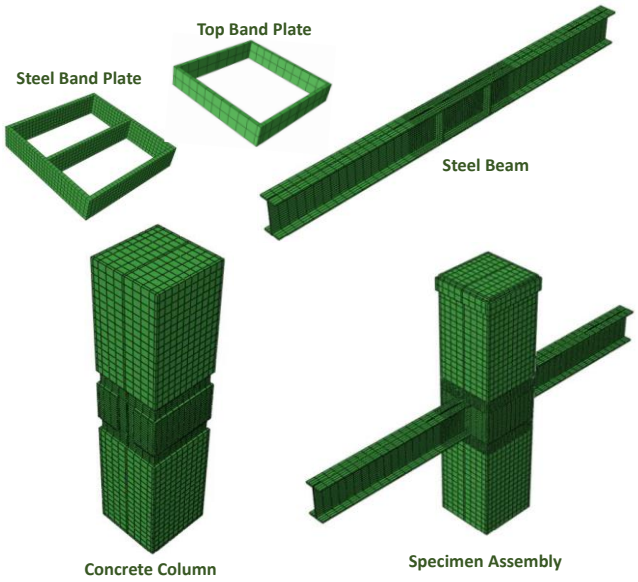

Fig. 13: Developed three-dimensional finite element model

3.3 Material Properties and Modeling

The modeled specimen incorporates all relevant interactions, boundary conditions, and material properties. Following test reports, ASTM A615 grade 75 [38] steel is used for longitudinal rebars, and ASTM A615 grade 60 [38] is employed for stirrups. The steel beam materials conform to ASTM A572 grade 50 [39]. The test results reveal a yield stress of 362.7 MPa and an ultimate strength of 495 MPa for the steel beam, while the mean compressive strength of concrete is measured at 50.8 MPa.

The model integrates the nonlinear properties of steel beams and rebars, utilizing an isotropic hardening model based on the von Mises yield criterion. The stress-strain relationships for the steel beams are established from results obtained in uniaxial tension tests. Concrete material is represented using the Concrete Damaged Plasticity model, which is available in the ABAQUS library. This model presupposes the primary failure mechanisms to involve tensile cracking and compressive crushing of the concrete material. The assumptions regarding this material model are derived from the validation study conducted by Tao et al. [36].

The concrete crack distributions are modeled using the total strain rotating crack model developed by Thorenfeldt [38]. The stress-strain relationship, as per Thorenfeldt's uniaxial compressive model,is illustrated in Fig. **14**(a) and defined as follows:

$$\sigma_c = f_c^{'} \frac{\varepsilon_c}{\varepsilon_0} \left(\frac{n}{n - \left(1 - (\frac{\varepsilon_c}{\varepsilon_0})^{nk} \right)} \right) \tag{16}$$

$$n = 0.8 + \frac{f_c^{'}}{17}, \quad k = \begin{cases} 1 & \varepsilon_0 \geq \varepsilon \\ 0.67 + \frac{f_c^{'}}{62} & \varepsilon_0 < \varepsilon \end{cases} \tag{17}$$

where ε_0 denotes the strain corresponding to the maximum compressive strength f'_c, determined in MPa as follows:

$$\varepsilon_0 = \frac{f_c^{'}}{E_c} \cdot \frac{n}{n-1} \tag{18}$$

$$E_c = 4700\sqrt{f_c^{'}} \tag{19}$$

The tension-crushing behavior is simulated by the tension-softening law suggested by Hordijk [40]. The stress-strain relationship, according to Hordijk's model, is depicted in Fig. **14**(b) and is described as follows:

$$\sigma_{cr} = f_t \left[\left(1 + (c_1 \frac{\varepsilon_{cr}}{\varepsilon_u})^3 \right) e^{-c_2 (\frac{\varepsilon_{cr}}{\varepsilon_u})} - \frac{\varepsilon_{cr}}{\varepsilon_u} (1 + c_1^3) e^{-c_2} \right] \tag{20}$$

where c_1 equals 3.0, and c_2 equals 6.9. The ultimate strain value, ε_u , i affected by the fracture energy G_f and the tensile strength f_t, and it is evaluated by Equation (21). The fracture energy G_f is determined using Equation (22) suggested by Remmel [41].

$$\varepsilon_u = 5.136 \frac{G_f}{h\, f_t} \tag{21}$$

$$G_f = 0.065 \cdot \ln\left(1 + \frac{f_c^{'}}{10} \right) \tag{22}$$

The crack bandwidth, denoted as *h*, serves as a characteristic length that reflects the mesh condition relative to the fracture energy G_f . *h* varies based on the dimensions of the solid concrete element, with the default value defined as $h = \sqrt[3]{V}$, where *V* signifies the volume of the element.

The unloading and reloading paths for tension and compression are simulated using a secant approach, as expressed in Equations (23) and (24), respectively, and are depicted in Fig. **15** Consequently, the model assumes that damage recovery is not possible, indicating significant

stiffness degradation. The secant approach cannot capture inelastic strain. This assumption aims to capture the pronounced pinching response observed in joints.

$$D_c = 1 - \frac{\sigma_c}{E_0 \varepsilon_c} \tag{23}$$

$$D_t = 1 - \frac{\sigma_{cr}}{E_0 \varepsilon_{cr}} \tag{24}$$

3.4 FE Model Validation

Fig. **16** compares the hysteretic response curves of the joints resulting from the experimental tests and FE analysis. As seen, the results of FE modeling are comparable to the experimental data in terms of initial stiffness, maximum strengths, and degradation in stiffness and strength in consecutive cycles. The simulated values for subsequent cycles align well with the experimental data. Nonetheless, discrepancies are noticeable during the initial cycles. This variance could be ascribed to the unevenness in the contact area between the actuator and the specimen. This unevenness diminishes the stiffness observed in the test specimens and is commonly identified as seating deformation in existing literature [22, 23].

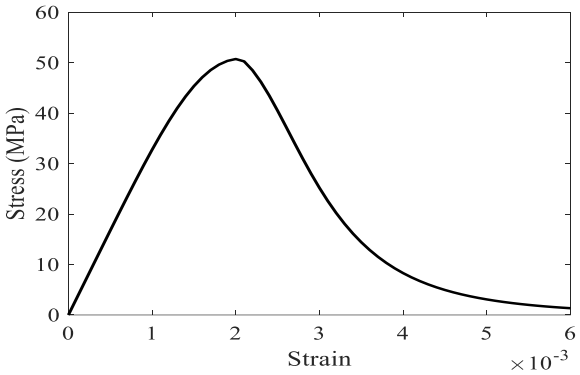

(a)

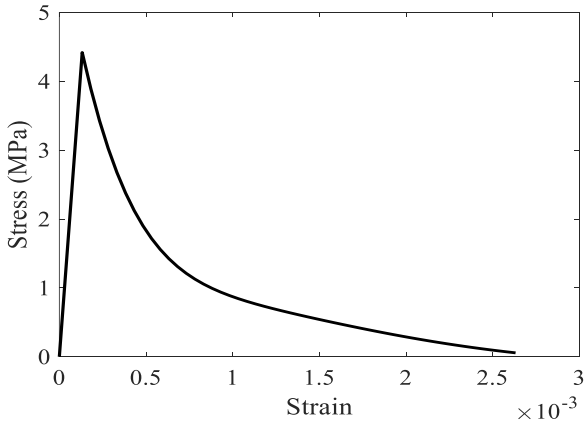

(b)

Fig. 14: Stress-strain relationship for concrete material: (a) under compression and (b) under tension

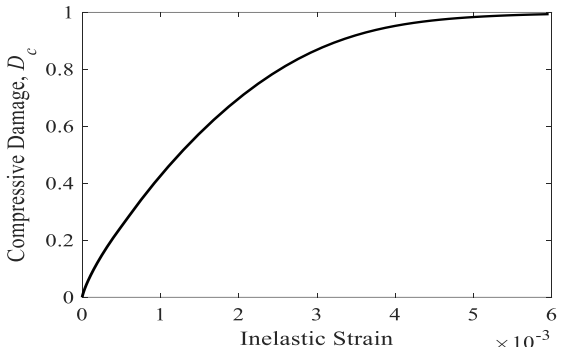

(a)

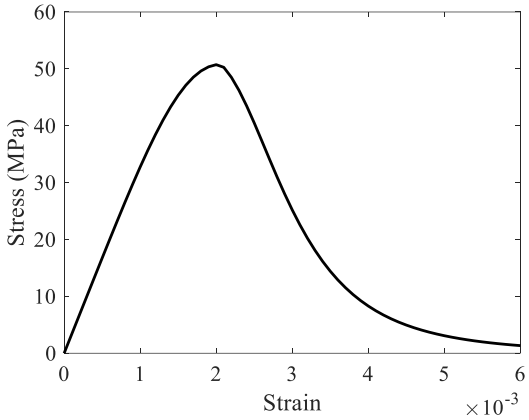

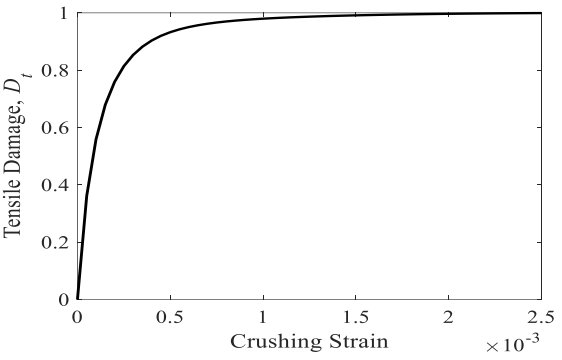

(b)

Fig. 15: Material model for concrete damage plasticity: (a) under compression and (b) under tension

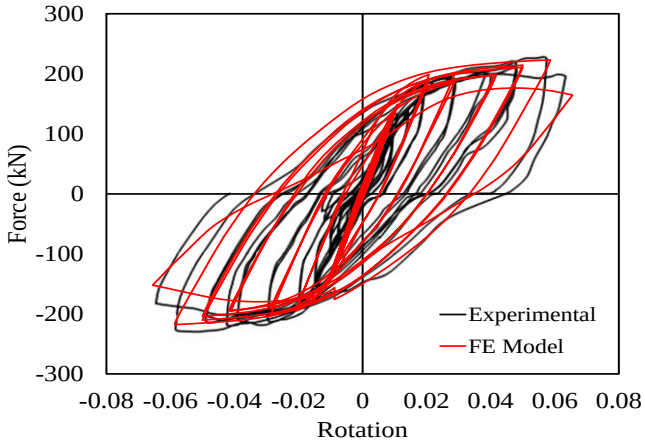

Fig. 16: Model validation through comparing the hysteretic curves resulted from experimental test and FE model

4. Details of Investigated Connections

This study investigates four through-beam type RCS connections. For each specimen, a numerical model is created in ABAQUS, following the validated modeling procedure outlined in Section 3, and then analyzed. The geometries of the models have been selected to comply with the specifications of the Structural Dynamics Strong Floor laboratory at Sharif University of Technology [20]. It is noteworthy that this study is a part of an ongoing numerical-experimental research program.

The specimens represent the half-scale of a typical RCS beam-column subassembly, comprising 1450 mm long RC columns and a continuous steel beam with a length of 2350 mm. The RC column has a cross-section with dimensions of 350 × 350 mm and concrete with a compressive strength of 30 MPa. The RC column includes 12 Φ12 longitudinal reinforcements and Φ10 @ 50- or 75-mm transverse reinforcements. Both longitudinal and transverse reinforcements are made of S400 steel material, complying with the 9th volume of the Iranian National Building Code (INBC) [42], and possess yield and ultimate strengths of 400 and 600 MPa, respectively. The steel beam has an IPE 200 section and is made of S235 (ST37) steel, conforming to the 10th volume INBC [43], with yield and ultimate strengths of 240 and 370 MPa, respectively.

Four chosen specimens consist of two designed according to the 1994 Guideline requirements and two according to the 2015 Pre-standard requirements. In each pair, the first specimen adheres to a common RCS joint detail approved by both design guidelines, featuring flange bearing plates, steel band plates with vertical stiffeners, and stirrups in the joint region. The second specimen in each pair is similar to the first but incorporates an additional four triangular stiffener plates attached to the outer corners of the connection to enhance joint stiffness. The primary objective of comparing these specimens is to assess the performance differences between connections designed according to the 1994 Guideline and the 2015 Pre-standard. An additional implicit goal is to explore the impact of four extra triangular stiffener plates on the overall performance of the connections.

The four selected specimens are defined as follows: the first and second specimens are designed in compliance with the 2015 Pre-standard, without, and with triangular stiffeners, respectively. The third and fourth specimens are designed according to the 1994 Guideline, without and with triangular stiffeners, respectively.

The geometric configuration of Specimen #1 is shown in Fig. **17**(a). In the joint area, three Φ10 stirrups with a 45 mm spacing are used. The joint stirrups pass through 12 mm holes in the steel beam web. Steel Band Plates with a height of 70 mm and a thickness of 12 mm are utilized. The Steel Band Plates are stiffened by two vertical stiffeners welded to the beam flanges above and below the steel beam. The vertical stiffeners have the same height as the Steel Band Plate, 7 mm, and a thickness of 10 mm. Face Bearing Plates have been included with the same width as the steel beam flange and a thickness of 12 mm. During the simulation, an axial load of 200 kN is applied to the top of the concrete column. For ease of implementation, longitudinal reinforcements in the entire length of the column are arranged in groups of three at each corner.

The configuration of Specimen #1 is considered as a basis for other specimens and minor changes are applied to it. So, the details of Specimen #2 are considered the same as Specimen #1 with the difference that an additional four triangular stiffener plates are attached to the outer corners of the connection. By summing up the widths of the inner and outer panels (bi + bo) for both specimens, the effective width of the joint within the column, bj, is determined as 217 mm and 175 mm according to the 2015 Pre-Standard and 1994 Guideline, respectively. The panel shear strength criterion, as per the 2015 Pre-Standard (Equation (6)), is satisfied, resulting in a demand-over-capacity ratio of 0.87. However, based on the 1994 Guideline (Equation (4)), this criterion is not met, yielding a ratio of 1.22. On the other hand, the 2015 Pre-Standard vertical bearing strength limit (Equation (7)) is not limiting. Moreover, based on the 1994 Guideline, the vertical bearing strength criterion (Equation (5)) is met, resulting in a ratio of 0.90.

The panel shear strength criterion of the 1994 Guideline can be met by incorporating a doubler plate with a thickness of 6 mm, resulting in a demand-over-capacity ratio of 0.95. Consequently, in Specimens #3 and #4, designed to comply with the 1994 Guideline, a doubler plate is utilized. Specimens #3 and #4 mirror Specimens #1 and #2, respectively, with the addition of a 6 mm thick doubler plate welded to the web of the steel beam in the joint zone. It is important to note that as the 1994 Guideline imposes stricter criteria than the 2015 Pre-standard, Specimens #3 and #4 also meet the requirements of the 2015 Pre-standard. The details of Specimens #1 to #4 are illustrated in Figure 8, and Table 1 provides a brief comparison of the key features of the four examined specimens.

Table 8: Comparison of the key features of the four examined specimens

Spec.No.	Beam Section	Column Section	Triangl. Stiffener Plate	Web Doubl. Plate	Meet 1994 Guideline?	Meet 2015 Pre-standard?
#1	IPE200	350×350 mm² 12Φ12	✗	✗	✗	✓
#2			✓	✗	✗	✓
#3			✗	✓	✓	✓
#4			✓	✓	✓	✓

5. Results and Discussions

Fig. **18** compares the force-displacement hysteresis curve for the selected specimens. Specifically, this figure compares (a) Specimens #1 vs. #2, (b) Specimens #3 vs. #4, (c) Specimens #1 vs. #3, and (d) Specimens #2 vs. #4. As discussed earlier, Specimens #3 and #4 are similar to Specimens #1 and #2, respectively, with the difference that a doubler plate with a thickness of 6 mm is attached to their beam web. This modification enables them to satisfy the requirements of both the 1994 Guideline and the 2015 Pre-standard, while Specimens #1 and #2 only meet the requirements of the 2015 Pre-standard. Moreover, Specimens #2 and #4 are similar to Specimens #1 and #3, respectively, with the difference that four triangular stiffeners are attached to the four outside corners of the joint to increase rigidity.

By examining Fig. **18**(a) and Fig. **18**(b), it can be observed that adding triangular stiffeners to the joint corners (i.e., Specimens #2 and #4) increases the connection strength in the initial and middle load cycles. However, in the end cycles when the deformation is high, the behavior of the two specimens converges. Additionally, the addition of triangular stiffeners is noted to enhance the initial stiffness

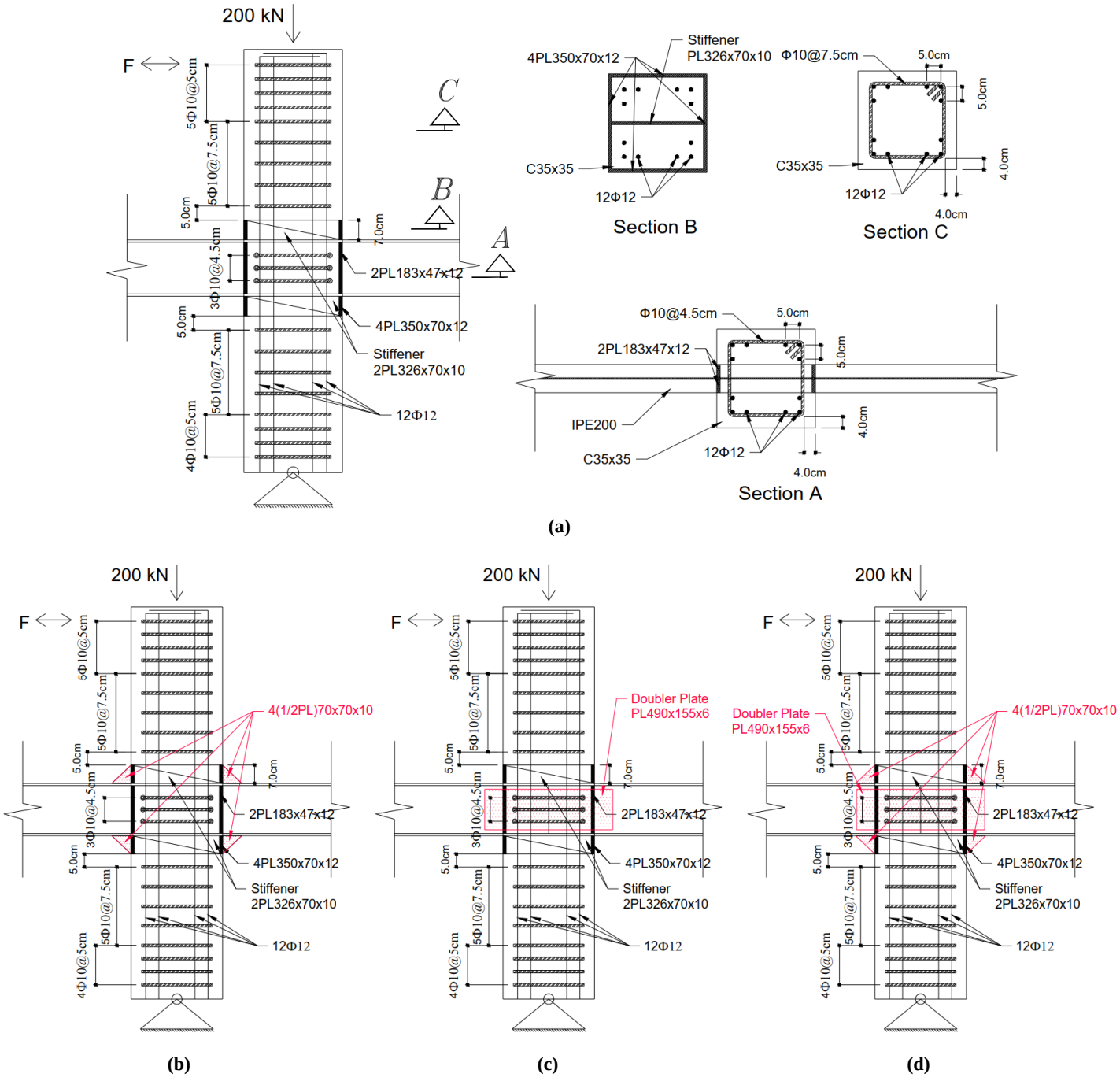

Fig. 17: Design details of the RCS connections evaluated in this study, (a) Specimen #1, (b) Specimen #2, (c) Specimen #3, and (d) Specimen #4

across almost all cycles. In other words, these stiffeners contribute to the increased robustness of the connection by augmenting its shear stiffness and initial strength.

Furthermore, upon examining Fig. **18**(c) and Fig. **18**(d), it becomes apparent that specimens meeting the requirements of the 1994 Guideline (i.e., Specimens #3 and #4) outperform those designed based on the 2015 Pre-standard. Specimens #3 and #4 exhibit higher initial strength and less strength degradation in successive load cycles compared to Specimens #1 and #2, respectively. It is crucial to note that this improved performance is solely achieved by adding a 6 mm doubler plate to the beam's web at the joint region.

Fig. **19** shows the backbone curve resulting from the hysteresis curve for the investigated connections in the backward (Fig. **19**(a)) and forward (Fig. **19**(b)) load directions separately. The forward load direction is considered as the left-to-right direction of loads, while the backward direction is considered as right-to-left. As observed in the figure, the weakest performance is associated with Specimen #1, and the best performance is seen with Specimen #4.

Specimen #2 (Specimen #1 + triangular stiffeners) demonstrates significantly improved performance in the range of low to medium deformation compared to Specimen #1. However, as deformation significantly increases (around a drift ratio of 6%), its performance diminishes, reaching a level comparable to Specimen #1 and even weaker than Specimen #1 in backward loading. Specimens #3 and #4 exhibit nearly consistent performance, with Specimen #4 showing slightly superior performance. Notably, Specimens #3 and #4, featuring a 6mm doubler plate compliant with both the 1994 Guideline and the 2015 Pre-standard, demonstrate markedly better performance in both load directions compared to Specimens #1 and #2, which comply only with the 2015 Pre-standard.

Fig. **20** compares the cumulative energy dissipated through plastic deformations in the investigated specimens. The amount of dissipated energy within each cycle is obtained

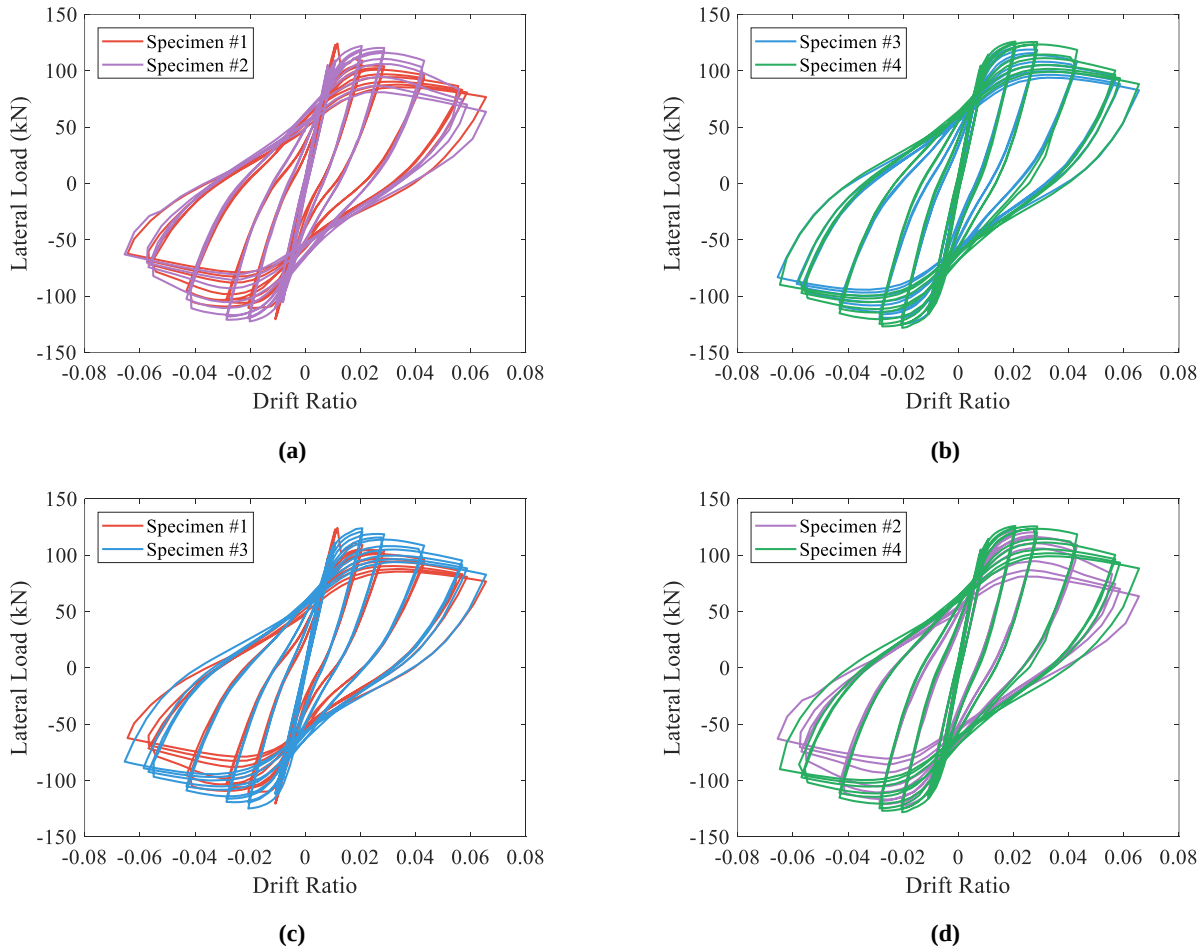

Fig. 18: Comparison of force-displacement hysteresis curve among investigated specimens (a) Specimens #1 vs. #2, (b) Specimens #3 vs. #4, (c) Specimens #1 vs. #3, and (d) Specimens #2 vs. #4

by calculating the area inside the hysteresis loops. It can be observed that, for all specimens, the energy dissipated in the initial 12 cycles (up to a drift of 1%) is minimal. In other words, within this range, all connections exhibit elastic behavior and do not undergo significant plastic deformation. Conversely, with an increase in deformation in the subsequent cycles, the energy due to external loads is dissipated through plastic deformations. The best performance is associated with Specimen #4. Interestingly, towards the end of the loading, the cumulative dissipated energy in Specimens #2 and #3 is nearly equal. In other words, in terms of total dissipated energy, adding triangular stiffeners to Specimen #1 is as effective as adding doubler plates to satisfy the requirements of the 1994 Guideline. The improvement in total energy dissipation in Specimen #4 compared to Specimen #1 is equal to 25.5%, while this improvement in Specimen #2 and #3 compared to Specimen #1 averages 12.2%.

Fig. **21** shows the stiffness degradation in successive cycles. Stiffness degradation in this context is defined as the ratio of effective stiffness in each cycle to the stiffness of the first cycle. It can be observed that cyclic stiffness degradation exhibits a similar pattern in all specimens. The degradation in stiffness initiates from the seventh cycle. In the final cycle for all specimens, the stiffness of all connections reaches approximately 8% of the initial stiffness. It is noteworthy that Specimen #1, which performs the weakest compared to other specimens, experiences a lesser stiffness drop in the intermediate cycles. However, this connection also undergoes similar degradation in the subsequent cycles as observed in other specimens.

Fig. **22** shows the strength degradation in successive cycles. In Fig. **22**(a), the strength degradation is depicted in the backward load direction (negative force and displacement in the hysteresis curve), while Fig. **22**(b) illustrates the strength degradation in the forward load direction (positive force and displacement in the hysteresis curve). As expected, Specimen #4 and Specimen #1 exhibit the best and worst performance, respectively. The strength degradation in Specimen #1 begins from the 12th cycle and continues significantly in subsequent cycles. On the other hand, Specimen #2 (Specimen #1 + triangular stiffeners) demonstrates a more stable and comparable performance compared to Specimen #4 up to the 16th cycle. However, this specimen also experiences a significant drop in strength in the subsequent cycles.

It is evident that the joints of Specimens #3 and #4, which meet the requirements of both the 1994 and 2015 guidelines, exhibit a more stable performance than Specimens #1 and #2. The ratio of shear strength in the last cycle (associated with drift of 6%) to the initial strength in Specimens #3 and #4 is obtained around 0.7, whereas this ratio is about 0.5 for Specimens #1 and #2. In other words, the connection performance in terms of cyclic loading strength degradation improved by up to 40%.

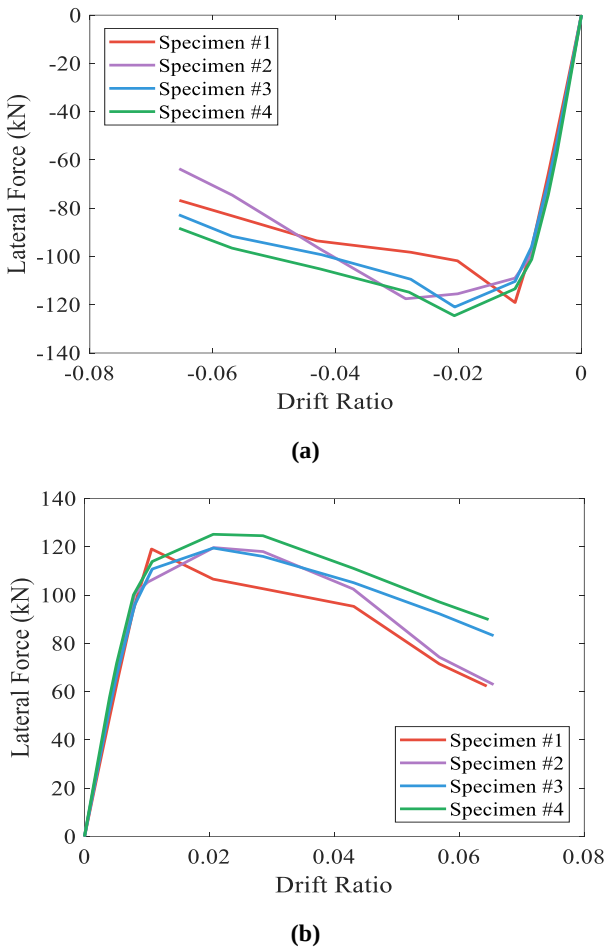

Fig. 19: Comparison of the backbone curve among investigated specimens (a) backward load direction and (b) forward load direction

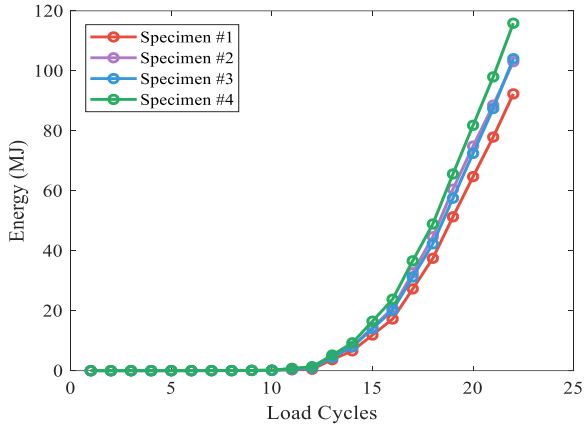

Fig. 20: Comparison of cumulative dissipated energy in successive cycles among investigated specimens

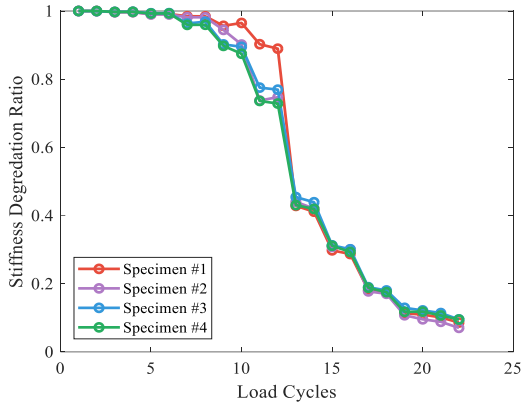

Fig. 21: Comparison of stiffness degradation in successive cycles among investigated specimens

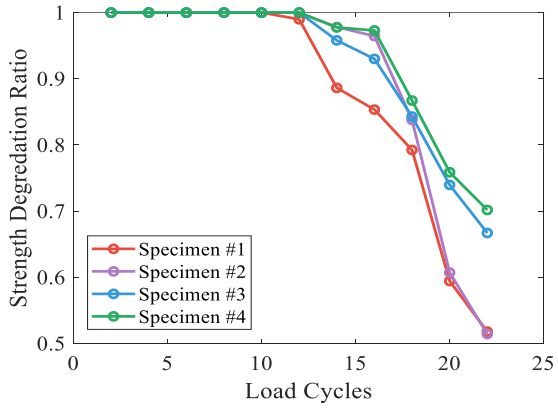

(a)

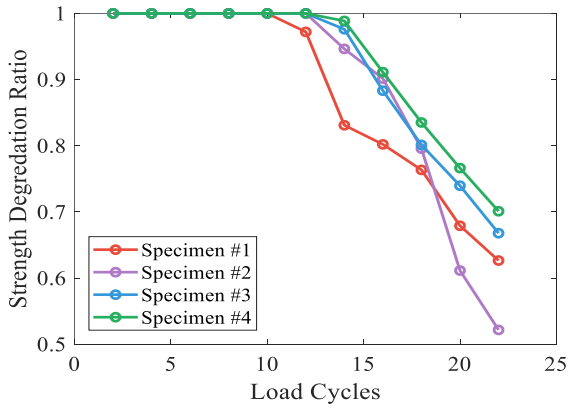

(b)

Fig. 22: Comparison of strength degradation in successive cycles among investigated specimens (a) backward load direction and (b) forward load direction

As a final remark, based on these observations, the incorporation of a doubler plate with a thickness of 6 mm, along with four triangular stiffeners measuring 70 × 70 × 10 mm, has significantly enhanced the seismic performance of the connection. This enhancement encompasses a 25.5% increase in the energy dissipation capacity of the connection and a 40% reduction in strength deterioration during cyclic loading. Notably, the addition of these accessories results in only a 3.7% increase in the steel usage of an RCS beam-column connection. Assuming that the construction cost of a steel moment-resisting frame constitutes approximately 10% of the building's total cost, these modifications contribute less than 0.5% to the overall building cost while substantially improving its seismic performance.

B ased on the findings of this study, it is noteworthy that one cannot conclusively assert that connections designed according to the requirements of the 2015 Pre-standard lack suitable seismic performance. All connections demonstrated nearly similar overall performance from certain perspectives. Instead, this study illustrates how the seismic performance of the connection can be effectively improved by incorporating extensions at a relatively low additional cost.

6. Conclusion

This study examined the performance of RCS connections conforming to the requirements outlined in the 1994 ASCE Guideline and the 2015 Pre-standard. Initially, a comparison was made between the shear strength criteria specified by each guideline. Generally, the 2015 Pre-Standard is less stringent than the 1994 Guideline. According to the 1994 Guideline, both panel shear and vertical bearing criteria must be concurrently satisfied. In contrast, the 2015 Pre-standard mandates only the fulfillment of the panel shear strength criteria in a more relaxed manner.

A comprehensive finite element model was developed and validated against previously experimental data. Next, a total of four specimens of RCS connections were selected for investigation. Finite element models were developed for each specimen, and then the models were analyzed under cyclic loading conditions. The four chosen specimens consist of two designed according to the 1994 Guideline requirements and two according to the 2015 Pre-standard requirements. In each pair, the first specimen adheres to a common RCS joint detail approved by both design guidelines, and the second is similar to the first but incorporates an additional four triangular stiffener plates attached to the outer corners of the connection to enhance joint stiffness. Specimens #1 and #2 are designated as specimens in compliance with the 2015 Pre-standard, without, and with triangular stiffeners, respectively. Specimens #3 and #4 are similar to Specimens #1 and #2, respectively, but to comply with the 1994 Guideline, a doubler plate with a thickness of 6 mm is attached to their beam web.

The main analysis results can be summarized as follows:

- The use of a 6 mm doubler plate in the joint region significantly improves initial strength, reduces strength

degradation, and enhances energy dissipation, particularly in Specimen #4.

- Triangular stiffeners contribute to increased initial stiffness and strength robustness at low to moderate deformation levels. Around a drift ratio of 6%, the performance of specimens with triangular stiffeners diminishes, converging to specimens without stiffeners.
- In terms of cyclic strength degradation, Specimens #3 and #4, complying with both the 1994 and 2015 guidelines, outperform Specimens #1 and #2, which are exclusively designed based on the 2015 Pre-standard. Specimens #3 and #4 exhibit a more stable performance, with up to 40% lower cyclic strength degradation at high deformation compared to Specimens #1 and #2, highlighting the effectiveness of adding a doubler plate to the web of the steel beam.
- In terms of total dissipated energy, adding triangular stiffeners is as effective as adding doubler plates. Specimen #4 had 25.5% more energy dissipation capacity than Specimen #1 and 11.9% more than Specimen #3, while this improvement in Specimen #2 and #3 compared to Specimen #1 averages 12.2%.

In conclusion, while further studies should be conducted to verify the results, this study demonstrates that the seismic performance of the connection can be significantly enhanced by incorporating just a 6 mm thick doubler plate and four triangular stiffeners. These modifications contribute less than 0.5% to the overall building cost. It is noteworthy that the findings of this study do not assert that connections designed according to the requirements of the 2015 ASCE lack suitable seismic performance. All specimens demonstrated nearly similar overall performance from certain perspectives. Instead, this study illustrates how the seismic performance of the connection can be effectively improved by incorporating extensions at a relatively low additional cost.

References

[1] G. G. Deierlein and H. Noguchi, "Overview of U.S.Japan Research on the Seismic Design of Composite Reinforced Concrete and Steel Moment Frame Structures," *J. Struct. Eng.*, vol. 130, no. 2, pp. 361–367, Feb. 2004, doi: 10.1061/(ASCE)0733-9445(2004)130:2(361).

[2] W. Li, Q. Li, W. Jiang, and L. Jiang, "Seismic performance of composite reinforced concrete and steel moment frame structures--state-of-the-art," *Compos. Part B Eng.*, vol. 42, no. 2, pp. 190–206, 2011.

[3] T. M. Sheikh, "Moment connections between steel beams and concrete columns.," The University of Texas at Austin, 1987.

[4] G. G. Deierlein, "Design of moment connections for composite framed structures.," The University of Texas at Austin, 1988.

[5] ASCE, "Guidelines for design of joints between steel beams and reinforced concrete columns," American Society of Civil Engineers, 1994.

[6] R. Kanno, "Strength, deformation, and seismic resistance of joints between steel beams and reinforced concrete columns.(Volumes I and II)," Cornell University, 1993.

[7] R. Kanno and G. G. Deierlein, "Seismic behavior of composite (RCS) beam-column joint subassemblies," in *Composite construction in steel and concrete III*, 1997, pp. 236–249.

[8] G. Parra-Montesinos and J. K. Wight, "Seismic Response of Exterior RC Column-to-Steel Beam Connections," *J. Struct. Eng.*, vol. 126, no. 10, pp. 1113–1121, Oct. 2000, doi: 10.1061/(ASCE)0733-9445(2000)126:10(1113).

[9] M. N. Bugeja, J. M. Bracci, and W. P. Moore Jr, "Seismic behavior of composite RCS frame systems," *J. Struct. Eng.*, vol. 126, no. 4, pp. 429–436, 2000.

[10] H. Noguchi and K. Kim, "Shear strength of beam-to-column connections in RCS system," in *Proceedings of Structural Engineers World Congress, Paper*, 1998.

[11] H. Kuramoto and I. Nishiyama, "Seismic Performance and Stress Transferring Mechanism of Through-Column-Type Joints for Composite Reinforced Concrete and Steel Frames," *J. Struct. Eng.*, vol. 130, no. 2, pp. 352–360, Feb. 2004, doi: 10.1061/(ASCE)0733-9445(2004)130:2(352).

[12] G. J. Parra-Montesinos, X. Liang, and J. K. Wight, "Towards deformation-based capacity design of RCS beam--column connections," *Eng. Struct.*, vol. 25, no. 5, pp. 681–690, 2003.

[13] G. G. Deierlein, G. Parra-Montesinos, P. Cordova, J. M. Bracci, and R. Kanno, "DRAFT - Pre-Standard for the Design of Moment Connections Between Steel Beams and Concrete Columns," 2015.

[14] ANSI/AISC 341, *Seismic Provisions for Structural Steel Buildings*. Chicago, IL: American Institute for Steel Construction, 2022.

[15] S. Alizadeh, N. K. A. Attari, and M. T. Kazemi, "The seismic performance of new detailing for RCS connections," *J. Constr. Steel Res.*, vol. 91, pp. 76–88, Dec. 2013, doi: 10.1016/j.jcsr.2013.08.010.

[16] S. Alizadeh, N. K. A. Attari, and M. T. Kazemi, "Experimental investigation of RCS connections performance using self-consolidated concrete," *J. Constr. Steel Res.*, vol. 114, pp. 204–216, Nov. 2015, doi: 10.1016/j.jcsr.2015.07.026.

[17] S. R. Mirghaderi, N. Bakhshayesh Eghbali, and M. M. Ahmadi, "Moment-connection between continuous steel beams and reinforced concrete column under cyclic loading," *J. Constr. Steel Res.*, vol. 118, pp. 105–119, Mar. 2016, doi: 10.1016/j.jcsr.2015.11.002.

[18] N. B. Eghbali and S. R. Mirghaderi, "Experimental investigation of steel beam to RC column connection via a through-plate," *J. Constr. steel Res.*, vol. 133, pp. 125–140, 2017.

[19] X. H. Nguyen, Q.-H. Nguyen, D. D. Le, and O. Mirza, "Experimental Study on Seismic Performance of New RCS Connection," *Structures*, vol. 9, pp. 53–62, Feb. 2017, doi:

10.1016/j.istruc.2016.09.006.

[20] A. Khaloo and R. Bakhtiari Doost, "Seismic performance of precast RC column to steel beam connections with variable joint configurations," *Eng. Struct.*, vol. 160, pp. 408–418, Apr. 2018, doi: 10.1016/j.engstruct.2018.01.039.

[21] R. B. Doost and A. Khaloo, "Steel web panel influence on seismic behavior of proposed precast RCS connections," in *Structures*, 2021, pp. 87–95.

[22] H. Chen, Z.-X. Guo, S. H. Basha, and Y. Liu, "Seismic behavior of RCS frame joints applied with high-strength bolts-end plate connection," *J. Build. Eng.*, vol. 63, p. 105455, 2023.

[23] J. Men, L. Xiong, J. Wang, Q. Zhang, and P. He, "An experimental study on the seismic behavior and replaceability of the replaceable steel shear links," in *Structures*, 2021, pp. 2334–2348.

[24] W. Li, H. Ye, Q. Wang, H. Liu, T. Ding, and B. Liu, "Experimental study on the seismic performance of demountable RCS joints," *J. Build. Eng.*, vol. 49, p. 104082, 2022.

[25] Y.-C. Ou, N. V. B. Nguyen, J. Joju, and J.-C. Wang, "Seismic behavior of concentric and eccentric New-RCS through-beam joints," *J. Build. Eng.*, vol. 76, p. 107357, 2023.

[26] Z. Pan, Q. Si, Y. Zhu, H. Ying, X. Wang, and D. Du, "Seismic performance of prefabricated semi-rigid RCS structures," in *Structures*, 2022, pp. 1369–1379.

[27] H.-J. Lee, H.-G. Park, H.-J. Hwang, and C.-S. Kim, "Cyclic Lateral Load Test for RC Column--Steel Beam Joints with Simplified Connection Details," *J. Struct. Eng.*, vol. 145, no. 8, p. 4019075, 2019.

[28] Dassault, "Abaqus Unified FEA," Paris, France, 2013. [Online]. Available: http://www.3ds.com/products-services/simulia/portfolio/abaqus/latest-release

[29] X. H. Nguyen, D. D. Le, and Q.-H. Nguyen, "Static behavior of novel RCS through-column-type joint: Experimental and numerical study," *Steel Compos. Struct.*, vol. 32, no. 1, pp. 111–126, 2019.

[30] W. Li, H. Ye, H. Liu, and B. Chen, "Development and testing of demountable RC column-to-steel beam connections under cyclic loading," *Soil Dyn. Earthq. Eng.*, vol. 159, p. 107342, 2022.

[31] N. Attari, N. Azadvar, S. Alizadeh, and others, "Numerical investigation of cover plate in RCS connections," *scientiairanica*, vol. 27, no. 1, pp. 10–24, 2020.

[32] S. Azad, S. R. Mirghaderi, and S. Epackachi, "Numerical investigation of steel and composite beam-to-encased composite column connection via a through-plate," in *Structures*, 2021, pp. 14–28.

[33] W. Li, Q. Li, and W. Jiang, "Parameter study on composite frames consisting of steel beams and reinforced concrete columns," *J. Constr. Steel Res.*, vol. 77, pp. 145–162, 2012.

[34] R. Madandoust, M. Vatandoost, and M. Zehtab, "Evaluation of seismic behavior improvement in RCS connections," *Asian J. Civ. Eng.*, vol. 19, no. 6, pp. 741–754, 2018.

[35] R. Bakhtiari Doost, H. Sadraie, A. Khaloo, and B. Badarloo, "Nonlinear finite element analysis and parametric study of executable RCS connections," *Arch. Civ. Mech. Eng.*, vol. 22, no. 4, p. 204, 2022.

[36] Y. Tao, W. Zhao, J. Shu, and Y. Yang, "Nonlinear Finite-Element Analysis of the Seismic Behavior of RC Column--Steel Beam Connections with Shear Failure Mode," *J. Struct. Eng.*, vol. 147, no. 10, p. 4021160, 2021.

[37] ANSI/AISC 360, *Specification for Structural Steel Buildings*. Chicago, IL: American Institute for Steel Construction, 2022.

[38] ASTM A615/A615M-12, "Standard specification for deformed and plain carbon-steel bars for concrete reinforcement," 2012.

[39] ASTM A572-15, "Standard specification for high-strength low-alloy columbium-vanadium structural steel," 2015.

[40] D. A. Horidijk, "Local approach to fatigue of concrete (PhD Thesis)," *Delft Univ. Technol. Netherlands*, 1991.

[41] G. Remmel, "Zum Zug-und Schubtragverhalten von Bauteilen aus hochfestem Beton," *Dtsch. Ausschußfür Stahlbet.*, no. 444, 1995.

[42] BHRC, "9th Volume of the Iranian National Building Code," Building and Housing Research Center, Tehran, Iran, 2020.

[43] BHRC, "10th Volume of the Iranian National Building Code," Building and Housing Research Center, Tehran, Iran, 2022.